Pulsed laser deposited indium tin oxides as alternatives to noble metals in the near-infrared region

OPEN ACCESS
IOP Publishing
Journal of Physics: Condensed Matter
J. Phys.: Condens. Matter **28** (2016) 224009 (10pp)
doi:10.1088/0953-8984/28/22/224009

Pulsed laser deposited indium tin oxides as alternatives to noble metals in the near-infrared region

Xu Fang[1,2], C L Mak[2], Shiyu Zhang[1], Zhewei Wang[1], Wenjia Yuan[1] and Hui Ye[1,3]

[1] State Key Laboratory of Modern Optical Instrumentation, Department of Optical Engineering, Zhejiang University, Hangzhou 310027, People's Republic of China
[2] Department of Applied Physics, The Hong Kong Polytechnic University, Hung Hom, Hong Kong, People's Republic of China

E-mail: huiye@zju.edu.cn

Received 4 May 2015, revised 4 September 2015
Accepted for publication 18 September 2015
Published 7 April 2016

Abstract

Transparent conductive indium tin oxide thin films with thickness around 200 nm were deposited on glass substrates by pulsed laser deposition technology. The microstructure and the electrical and optical properties of the ITO films deposited under different oxygen pressures and substrate temperatures were systematically investigated. Distinct different x-ray diffraction patterns revealed that the crystallinity of ITO films was highly influenced by deposition conditions. The highest carrier concentration of the ITO films was obtained as 1.34×10^{21} cm^{-3} with the lowest corresponding resistivity of 2.41×10^{-4} Ω cm. Spectroscopic ellipsometry was applied to retrieve the dielectric permittivity of the ITO films to estimate their potential as plasmonic materials in the near-infrared region. The crossover wavelength (the wavelength where the real part of the permittivity changes from positive to negative) of the ITO films exhibited high dependence on the deposition conditions and was optimized to as low as 1270 nm. Compared with noble metals (silver or gold etc), the lower imaginary part of the permittivity (<3) of ITO films suggests the potential application of ITO in the near-infrared range.

Keywords: indium tin oxide, deposition conditions, optical and electrical properties, plasmonic property

(Some figures may appear in colour only in the online journal)

1. Introduction

In general, among various metals gold (Au) and silver (Ag) are exclusively used as fundamental plasmonic materials for their extremely high carrier concentration N (~10^{22} cm^{-3}). Such a high carrier concentration contributes to a large plasma frequency (ω_p), which offers the possibility of generating surface plasmon polaritons at the interface between metals and dielectric surroundings in the visible range. Many applications such as biosensors [1–3], metamaterials [4–6], SPP waveguides [7] and nano-antennas [8] were based on the plasmonic property of noble metals. However, some drawbacks, such as nonadjustable optical and electrical properties, vulnerable chemical and mechanical stability [9, 10] and large magnitudes of the real part and imaginary part of the permittivity [11–13] of noble metals have hindered the design of devices for different uses, especially when the operating wavelength is located in the near-IR range. A technical problem which has challenged the integration of metals with the standard CMOS

[3] Author to whom any correspondence should be addressed.

process is the diffusion of metals into silicon as dopant or contamination [14, 15]. All the mentioned disadvantages hinder the further development of metals in the field of plasmonics, and these are also the factors that motivate researchers to discover alternative candidates to noble metals.

With the unique property of high carrier concentration (~10^{21} cm^{-3}) [16, 17], transparent conductive oxides (TCOs) have also attracted researchers' attention as plasmonic materials in the near-infrared (IR) range despite their traditional roles as transparent electrodes in the panel display and photovoltaic industry. Advantages of TCOs [18–22] over noble metals or competitors such as titanium nitride (TiN) [23–25] as plasmonic materials are various: properties can be manipulated according to deposition conditions [26, 27]; the relatively small magnitude of the real and imaginary parts of the permittivity (low loss); they are compatible with the standard CMOS fabrication process [28].

The most popularly used TCO is indium tin oxide (ITO) for its ability to offer the lowest resistivity (around 1–2 $\times$ 10^{-4} Ω cm) [16, 17]. Meanwhile, competitors, particularly doped zinc oxide (dopants such as Al, Ga etc), have emerged as alternatives to TCO for the sake of low cost and abundant availability. However, the conductivity of doped ZnO was not high enough compared with ITO: for Al:ZnO the reported resistivity was 3–4 $\times$ 10^{-4} Ω cm [26], the resistivity of Ga:ZnO [29] was around 2.8 $\times$ 10^{-4} Ω cm and so on. As a result, many applications have applied ITO as an effective plasmonic material. Some examples are the following. Franzen *et al* [20, 30–32] explored the plasmonic property of ITO films based on prism coupling and compared it with noble metals. Melikyan *et al* [33] successfully realized an absorption modulator (operation speed $>$ 100 Gbit s^{-1}) by changing the SPP absorption of the ITO layer at communication wavelength. Kim *et al* [34] systematically investigated the plasmonic resonances in nanopatterned TCOs (ITO, GZO, AZO) and confirmed that ITO can support SPPs at communication wavelength. Feigenbaum *et al* [35] altered the optical property of ITO by electronically changing the carrier concentration of the ITO layer in order to realize a plasmonic waveguide structure.

The evidence above shows promising potential for TCOs, particularly ITO, as important materials in the design of plasmonic or metamaterial devices. However, a problem that should not be ignored is that most of the optical properties of ITO used in the mentioned applications were based on theoretical reports or incomplete experimental parameters. Despite the fact that countless papers were about optimizing the deposition conditions to obtain excellent visible transparency and conductivity, reports had seldom been published to explore the relations between metallic behaviors of ITO in the near-IR range or plasmonic properties and the deposition conditions. In this paper, we deposited ITO films via the PLD technique and systematically investigated the optical and electrical properties as a function of the deposition conditions in the near-IR range. A spectroscopic ellipsometry measurement was made to retrieve the permittivity of the ITO films. Thorough characterizations of the ITO films with different plasmonic behaviors in the near-IR range are provided as references for the requirements of different plasmonic applications.

2. Experiment

The fabrication of the ITO films was completed through a PLD system whose KrF excimer laser source was a Compex Pro 205 (Coherent) with a laser wavelength of 248 nm and pulse duration of 20 ns. Prior to deposition the chamber was evacuated to below 2 $\times$ 10^{-3} Pa and then the target was ablated by the laser for 10 min. During deposition, the laser with 300 mJ power and 5 Hz repetition was 45° focused through a 50 cm focal length quartz glass onto a rotating target (10 revolutions min^{-1}) to avoid surface deterioration. The target–substrate distance was kept at 4 cm. The focused laser spot was a rectangular shape with an area of 0.4 $\times$ 0.5 cm^2, thus the ablation energy density was 1.5 J cm^{-2}. The ITO target (purity 99.99%) was a 2 in diameter and 5 mm thick ceramic disk with the composition of In_2O_3:SnO_2 = 90%:10% by weight. The substrates were 10 mm $\times$ 10 mm Corning Eagle XG AMLCD glass with thickness of 0.7 mm. The glass substrates were subsequently ultrasonically cleaned in acetone, methanol and distilled water for 10 min and were immediately dried with dry flowing nitrogen. When the chamber was evacuated to below 2 $\times$ 10^{-3} Pa, the substrate temperature was set and kept to a desired value (100–400 °C), after which oxygen could be injected into the chamber. By tuning the turbo pump valve and the gas valve, the ambient oxygen gas pressure of the deposition chamber was monitored at a constant level (1–10 Pa). After the deposition, the substrate was naturally cooled in the same oxygen conditions without any post-annealing process.

The crystallinity of the ITO films was explored through x-ray diffractometry (XRD, PANalytical X'Pert PRO, Cu Kα radiation). The thickness and the surface smoothness were investigated through field emission scanning electron microscopy (FESEM, Zeiss Ultra-55). Hall measurement (Ecopia, HMS-5000) was performed to obtain the carrier concentration, resistivity and Hall mobility of the ITO films using the van der Pauw configuration. The optical properties (direct transmittance) ranging from 300 nm to 2500 nm were measured with a Shimadzu UV-3101 spectrophotometer. The absorption (from 900–2500 nm) of the ITO films was calculated by measuring the reflectance and transmittance using Fourier transform infrared spectroscopy (FTIR: Bruker Vertex 70). Spectroscopic ellipsometry (Semilab GES 5E) was applied to measure the polarization change (quantified by the amplitude ratio, ψ, and the phase difference, Δ) when incident radiation interacted with ITO films. Then software (WinElli II) was used to retrieve the ITO films' optical permittivity (real part (ε') and imaginary part (ε'')) by fitting the measured data to a physical model in the range of 1000–2000 nm.

3. Results and discussion

The microstructure and crystallinity were explored through XRD measurement as shown in figure 1. According to the diffraction patterns (θ/2θ), it seemed that the microstructures of ITO films were highly dependent on the substrate temperature (T_s) and oxygen pressure (P_{O2}). The diffraction peaks of (2 1 1), (2 2 2), (3 3 2), (4 0 0) etc represented the ITO films' polycrystalline structure with high T_s. The positions of the peaks such

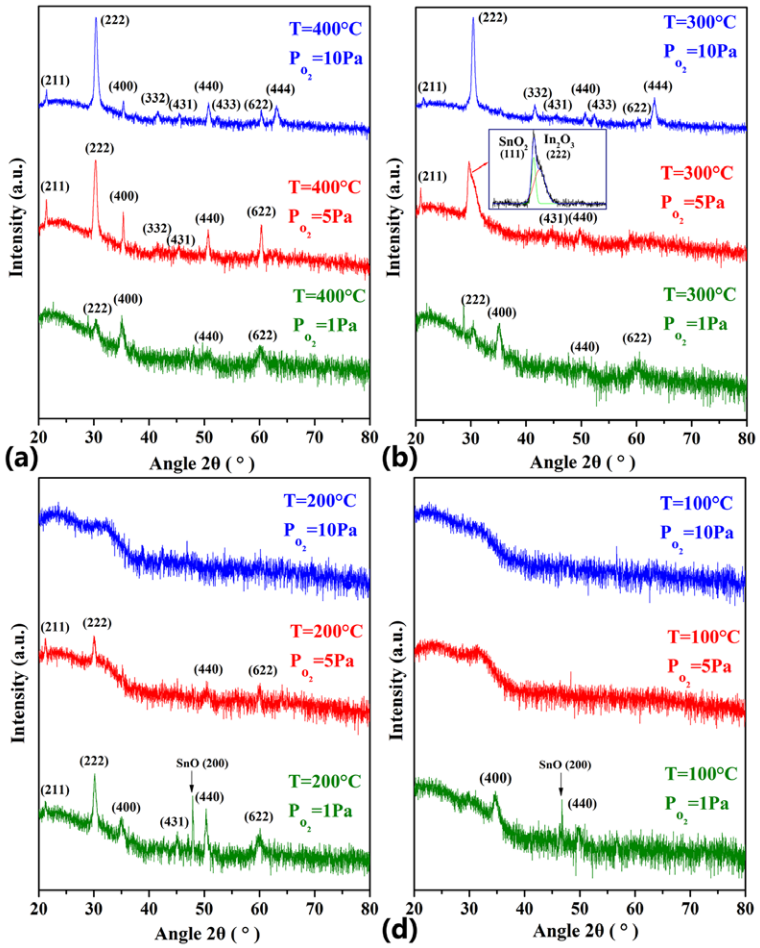

Figure 1. XRD pattern of ITO films deposited under different conditions. (a)–(d) ITO films deposited with substrate temperatures of 400 °C, 300 °C, 200 °C and 100 °C, respectively. Within each figure, blue, red and green lines represent films deposited under oxygen pressures of 10 Pa, 5 Pa and 1 Pa, respectively. The inset of (b) is the peak separation of SnO_2(1 1 1) and In_2O_3(2 2 2) phases of the ITO film.

as (2 2 2) at 30.3°, (4 0 0) at 35.3°, (4 4 0) at 51° etc were all consistent with that in In_2O_3 (JCPDS card no 06-0416) and the literature [36–39], meaning that the Sn^{4+} was substitutionally incorporated into the In^{3+} site or in the interstitial positions (except the likely SnO phase separation in figures 1(c) and (d) at 47°). However, when $T_s = 100$ °C in figure 1(d), the broad band in the patterns without any peaks showed that ITO films deposited with oxygen pressure of 5–10 Pa had an amorphous property. Only when oxygen pressure dropped to 1 Pa did the crystallinity start to form with (4 0 0) preferred orientation. Such a phenomenon could also be observed in the XRD patterns of ITO films deposited with $T_s = 200$ °C. The effect of oxygen partial pressure on the microstructure can be explained by the properties of PLD [40–42]; this was fully discussed by Kim *et al* [43].

Regardless of ambient oxygen pressure, all the ITO films with $T_s = 300$–400 °C possessed high polycrystallinity and exhibited nearly the same preferred orientation as shown in figures 1(a) and (b). The differences between patterns of ITO films with $T_s = 300$ °C and 400 °C indicated that the higher substrate temperature contributed to a higher degree of crystallinity. The peak around 30° of the $T_s = 300$ °C and $P_{O2} = 5$ Pa XRD pattern can be separated into SnO_2 (1 1 1) at 29.9° and In_2O_3 (2 2 2) phases according to SnO_2 (JCPDS card no 29-1484); such an observation was also reported by Petukhov *et al* [44]. Table 1 exhibits the ratio of (2 2 2) peak intensity versus that of the (4 0 0) peak (I[(2 2 2)/(4 0 0)]) to present the predominant orientation, and the approximate grain size calculated using the Scherrer equation [39]. From the evolution of the I[(2 2 2)/(4 0 0)] value, it was obvious to conclude that the ITO films' preferential orientation shifted from the (2 2 2) to the (4 0 0) crystallographic plane. The shrinking (2 2 2) linewidth in figure 1(a) echoes the growth of the calculated grain size, showing that higher oxygen pressure led to larger grain size [39, 43].

Figures 2(a)–(c) are the FESEM cross-sections of ITO films on glass substrates deposited under a constant T_s of 400 °C and P_{O2} of 10 Pa, 5 Pa and 1 Pa, respectively. The ITO films deposited at T_s =300 °C and $P_{O2} = 1$ Pa are also shown in figure 2(d) for comparison. All the films exhibited excellent thickness uniformity and sharp edges owing to the unique ability of the PLD technique to fabricate high quality thin films. The thicknesses of the ITO films were controlled by deposition duration. From the details of the cross-sections, all the films exhibited textured cross-sections with packed nano-column structures (nearly vertical to the surface of the substrate), which were similar to reported results [45]. The identical XRD patterns for $P_{O2} = 1$ Pa, T_s =400 °C, and

Table 1. Evolution of the calculated grain size and the ratio of (222) phase peak intensity versus (400) phase peak intensity as a function of oxygen pressure.

Oxygen pressure (Pa)	Thickness (nm)	I[(222)/(400)]	Grain size (nm)	N (cm^{-3})	ρ (Ω cm)	μ ($cm^2\ V^{-1}\ s^{-1}$)	$R_{\square}$ ($\Omega\ \square^{-1}$)
10	200.5	49.6	27	2.85×10^{20}	6.03×10^{-4}	36.3	23.3
5	223.4	5.2	17.8	6.96×10^{20}	2.59×10^{-4}	34.6	12.2
1	220.5	0.75	10.86	1.34×10^{21}	2.41×10^{-4}	19.4	14.6

The corresponding electrical parameters including carrier concentration (N), resistivity (ρ), sheet resistivity (R) and Hall mobility (μ) were measured. The substrate temperature was kept at 400 °C while the oxygen pressure was variable.

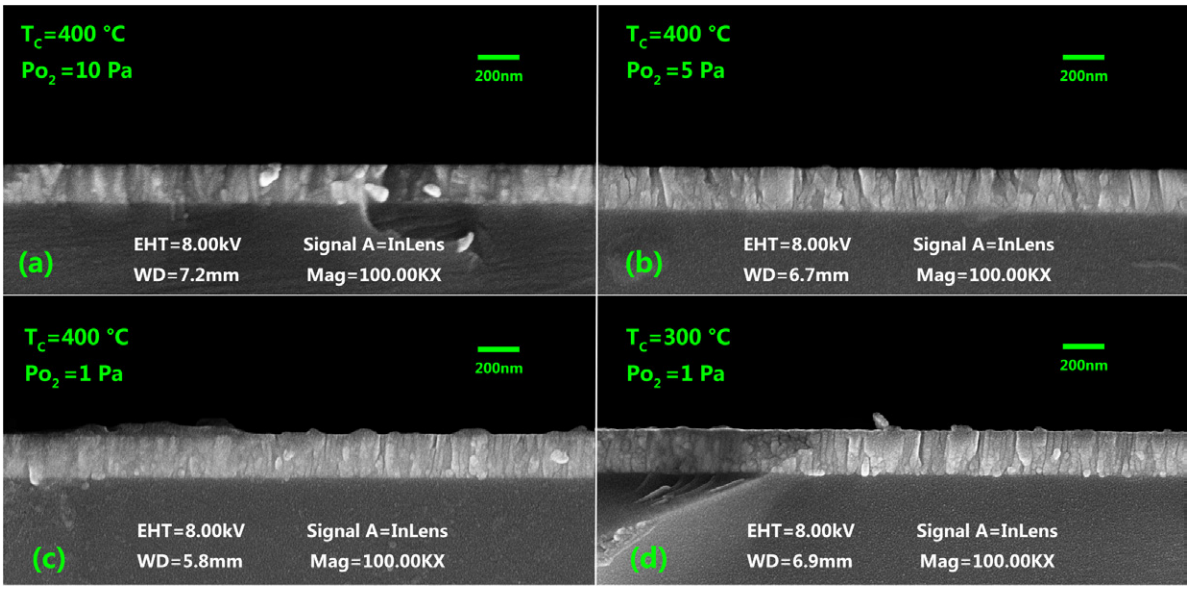

Figure 2. SEM cross-section images of ITO films as a function of deposition conditions: substrate temperature (T_s) and oxygen pressure (P_{O2}). (a) $T_s = 400$ °C, $P_{O2} = 10$ Pa; (b) $T_s = 400$ °C, $P_{O2} = 5$ Pa; (c) $T_s = 400$ °C, $P_{O2} = 1$ Pa, (d) $T_s = 300$ °C, $P_{O2} = 1$ Pa.

$P_{O2} = 1$ Pa, $T_s = 300$ °C, reflected the similar nano-structures in figures 2(c) and (d). When T_s was fixed at 400 °C, we can observe that the average width of nano-columns narrowed and they became more condensed and compacted according to the decreased ambient oxygen gas pressure. This also echoes the results revealed by XRD patterns: the calculated grain sizes in table 1 increased as oxygen pressure rose.

Hall measurements with the van der Pauw configuration of four probes were made to obtain the electrical parameters. In figure 3, carrier concentration (N), resistivity (ρ), sheet resistance ($R_{\square}$) and Hall mobility (μ) depending on substrate temperature were measured and illustrated as black squares (■), red triangles (▲), green stars (☆) and blue dots (●), respectively. The carrier concentration exhibited a monotonic increase as T_s rose from 100 °C to 400 °C. The highest carrier concentration reached 1.34×10^{21} cm^{-3} when $T_s = 400$ °C; this carrier concentration was of the same magnitude as that of epitaxy grown ITO film (1.9×10^{21} cm^{-3}) [27, 46]. The Hall mobility linearly increased from 7.62 $cm^2\ V^{-1}\ s^{-1}$ to 19.4 $cm^2\ V^{-1}\ s^{-1}$ when T_s altered from 100 to 400 °C. In contrast, the resistivity and the sheet resistance shrank according to the increase of T_s. The minimum resistivity was $2.41 \times 10^{-4}\ \Omega$ cm at $T_s = 400$ °C and the corresponding sheet resistance was 14.6 $\Omega\ \square^{-1}$. The gradual increase of the carrier concentration was in agreement with others' research [36, 39]

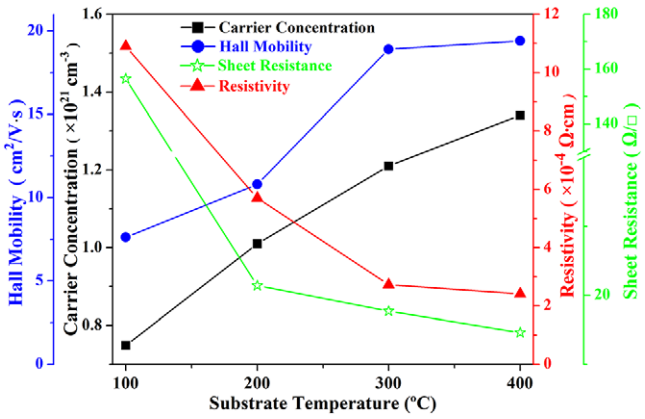

Figure 3. Variation of ■ carrier concentration (N), ● Hall mobility (μ), ▲ resistivity (ρ) and ☆ sheet resistance (R) with changing substrate temperature. The oxygen pressure was kept constant at 1 Pa.

and can be attributed to the diffusion of Sn atoms into the In cations [43]. In the meantime the decrease of resistivity (or sheet resistance) and increase of Hall mobility both benefited from the improved crystallinity of the ITO films introduced by the upgraded substrate temperature, as the reduction of grain boundaries (acting as traps or defects hindering the transition of electrons) would effectively improve the conductivity of the materials.

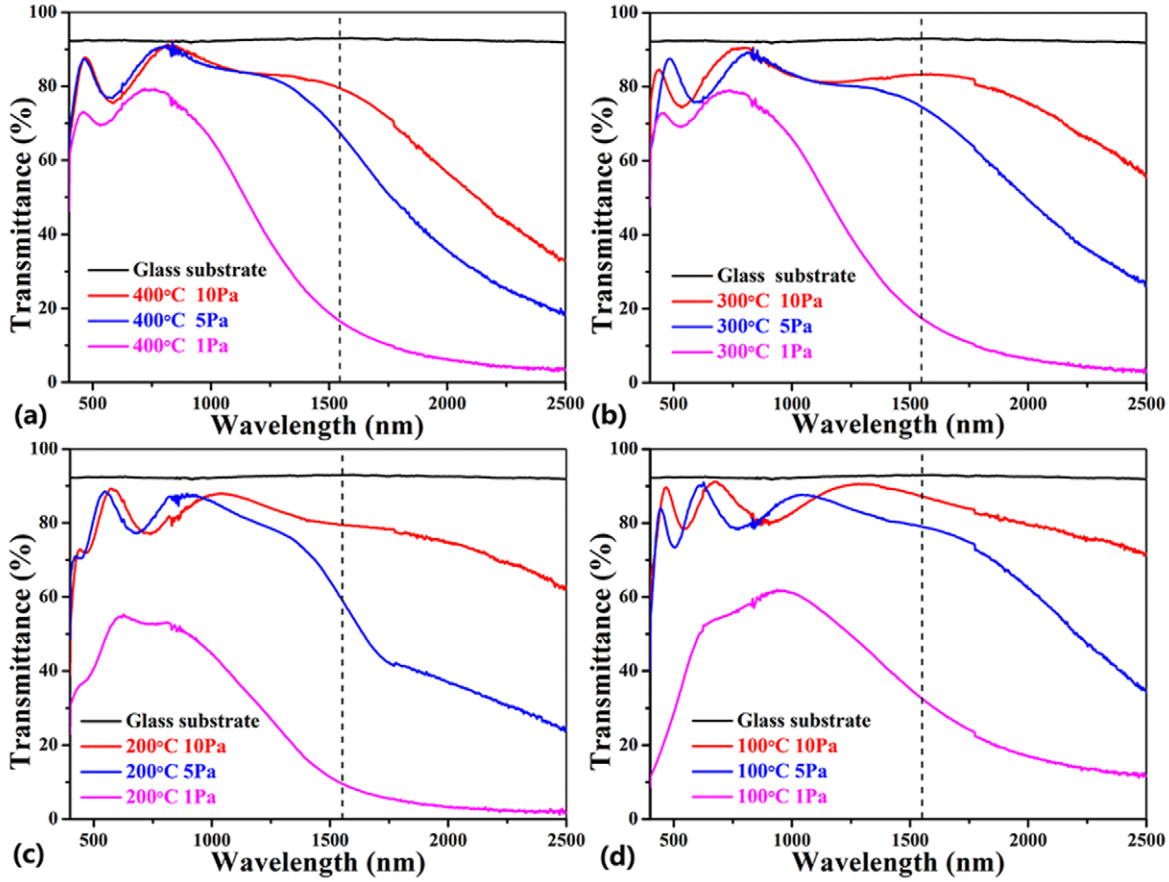

Figure 4. Incident transmittance (400–2500 nm) of ITO films deposited by PLD technology as a function of deposition conditions. (a)–(d) Substrate temperatures of 400 °C, 300 °C, 200 °C, and 100 °C, respectively. Within each figure, black, red, blue and green lines represent the transmittance of bare glass substrate and ITO films deposited under oxygen pressures of 10 Pa, 5 Pa and 1 Pa, respectively.

Table 1 provides the electrical properties (N, ρ, $R_{\square}$ and μ) of ITO films as a function of ambient gas pressure, when $T_s = 400$ °C. Another main factor contributing to the conductivity of TCOs was the existence of oxygen vacancies, as each oxygen vacancy was capable of creating two extra free electrons [39]. Consequently, the carrier concentration rocketed from 2.85×10^{20} to 1.34×10^{21} cm^{-3} when P_{O2} decreased from 10 Pa to 1 Pa. As expected, the resistivity decreased from 6.03×10^{-4} to 2.41×10^{-4} Ω cm as P_{O2} changed from 10 Pa to 1 Pa. Attention should be paid to the variation of Hall mobility: at first the mobility slightly decreased from 36.3 cm^2 V^{-1} s^{-1} to 34.6 cm^2 V^{-1} s^{-1} and then sharply dropped to 19.4 cm^2 V^{-1} s^{-1} as oxygen pressure changed from 10 Pa to 1 Pa. The decrease of Hall mobility can be blamed for the deterioration of crystallinity resulting from the excess number of oxygen vacancies, as can be seen from figure 1(a). Also the decrease of grain size would result in an increase of grain boundaries, which would hinder the transitions of electrons. Still, it was a compromise between obtaining high carrier concentration and high electron mobility.

Figures 4(a)–(d) are the direct transmittance (from 400–2500 nm) of the ITO films (~200 nm) deposited with substrate temperature from 400 °C to 100 °C. Within each panel, the black solid line (overall transmittance of 92.3%) represents the high transparency of bare Corning glass substrate without any deposited films. Lines colored red, blue and green are the transmittances of ITO films deposited with different P_{O2} values of 10 Pa, 5 Pa and 1 Pa, respectively. The peaks and valleys in the visible range (400–800 nm) of each line are due to the thin film interference effect, which is a common phenomenon.

It was clearly observed that, when the substrate temperature was kept constant, the ITO films possessed higher overall transparency if P_{O2} was higher. Furthermore, the differences of transmittance between different oxygen pressures enlarged as the wavelength increased from the visible range to wavelengths above 1000 nm. In figure 4, the dashed lines located at the wavelength of 1550 nm are drawn to manifest the optical behaviors of ITO films in the near-IR range. For $T_s = 400$ °C in figure 4(a), the transmittances at 500 nm of ITO films deposited with P_{O2} values of 10 Pa, 5 Pa and 1 Pa were 84.6%, 83.3% and 70.9%, respectively, while as the wavelength increased to 1550 nm the corresponding transmittances decreased to 80%, 67% and 16.4% accordingly. Moreover, the ITO film with $P_{O2} = 10$ Pa exhibited a broad band of high transparency (>80%) from 400 nm to 1600 nm. However, the transparent window of the ITO film with $P_{O2} = 5$ Pa shrank to the range of 400–1300 nm; furthermore, the transmission window for the ITO film with $P_{O2} = 1$ Pa severely narrowed to 400–1000 nm. The gradual decrease of transmittance in the

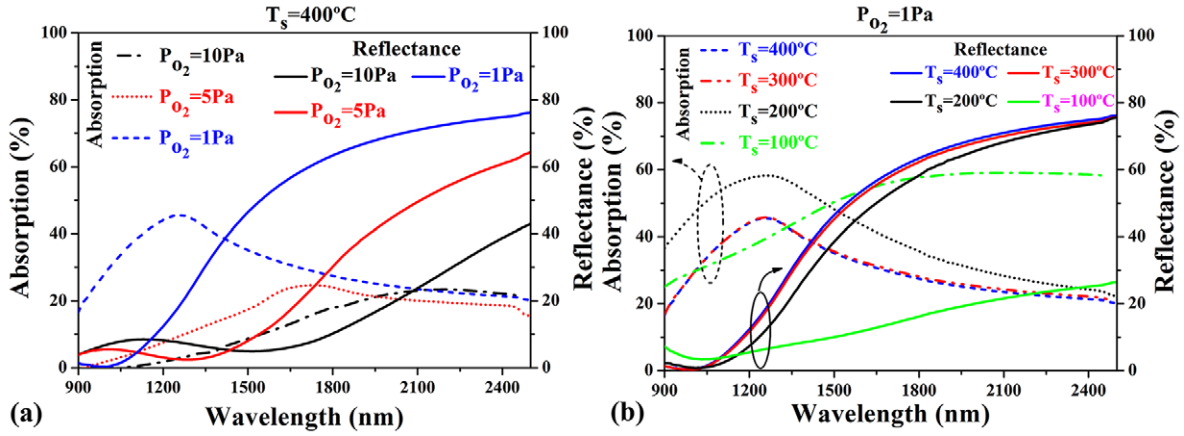

Figure 5. The absorption and reflectance (measured using FTIR) of ITO films as a function of substrate temperature and oxygen pressure. (a) Absorption (broken lines) and reflectance (solid lines) of ITO films deposited with 10 Pa (black), 5 Pa (red) and 1 Pa (blue) oxygen pressure; the substrate temperature was kept constant at 400 °C. (b) Absorption (broken lines) and reflectance (solid lines) of ITO films deposited with substrate temperatures of 400 °C (blue), 300 °C (red), 200 °C (black) and 100 °C (green); the oxygen pressure was 1 Pa.

near-IR range and the narrowing of the transparent window were mainly due to the free carrier plasma resonance located in the near-IR range [47–49]. The free electrons oscillated with incident light with a specific frequency and screened the electromagnetic wave via intraband transitions within the conducting band [16, 47]. According to the Drude model [39, 47], the plasma frequency ω_p was defined as follows:

$$\omega_p = \sqrt{\frac{Ne^2}{\varepsilon_\infty \varepsilon_0 m^*}} \quad (1)$$

where N is the carrier concentration, ε_∞ the high frequency dielectric constant, ε_0 the free space dielectric constant, e the electronic charge and m^* the effective mass of an electron. From equation (1), the plasma frequency ω_p was positively proportional to $\sqrt{N}$; consequently, the plasma frequency ω_p would exhibit a blue shift once the carrier concentration rose. For ITO film deposited with $T_s = 400$ °C and $P_{O2} = 10$ Pa the carrier concentration was 2.85×10^{20} cm^{-3}, and as P_{O2} decreased to 1 Pa the carrier concentration rocketed up to 1.34×10^{21} cm^{-3}. As a result, the increased carrier concentration was held responsible for making the IR transparent end shift to shorter wavelength.

The transmittance of ITO films was also influenced by the substrate temperature as well. When $P_{O2} = 10$ Pa, it seemed that the transparency of ITO films changed little, with a maximum value of around 90% in the visible range (400–800 nm) regardless of the T_s increase from 100 °C to 400 °C. However, the differences emerged in the near-IR range: the transmittances of ITO films with $T_s = 400$ °C at 1550 nm and 2500 nm were 79.36% and 33.19%. This transmittance increased with decreasing T_s: when $T_s = 100$ °C, the transmittances at 1550 nm and 2500 nm were 87.37% and 71.29%, which were the highest among all the samples. However, the carrier concentration (2.85×10^{20} cm^{-3}) of the ITO film deposited at $T_s = 400$ °C was much higher than that (2.44×10^{19} cm^{-3}) of the ITO film deposited at $T_s = 100$ °C. By combining the electrical property and optical measurement results, a trade-off should be taken into consideration between high transmittance and high conductivity.

In order to further inspect the influence of deposition conditions on the optical properties of ITO films, the reflectance in the range of 900–2500 nm was measured and presented in figure 5. The absorption was calculated using the relation $A = 1 - T - R$; T represents the transmittance, which was also measured using FTIR. Figure 5(a) exhibits the reflectance (solid lines) and absorption (broken lines) of ITO films as a function of oxygen pressure; the substrate temperature was fixed at 400 °C. From figure 5(a), the reflectance of the ITO films obviously increased linearly along with the enlargement of wavelength, and higher carrier concentration would bring higher reflectance, especially at longer wavelength. Such a phenomenon echoes the results of lowered transmittance with higher carrier concentration shown in figure 4(a). Accordingly, the absorption lines presented three remarkable points: (1) the absorption peak narrowed or the half-width of the absorption band deceased with increasing carrier concentration; (2) the center wavelength of the absorption peak shifted to shorter wavelength (blue shift occurred when substrate temperature was constant, the oxygen pressure decreased); (3) the absorption intensified with increasing carrier concentration. The wavelength where the absorption reached a maximum was usually regarded as the plasma frequency λ_p [39, 47]. λ_p shifted to 1260 nm when the carrier concentration reached its maximum of 1.34×10^{21} cm^{-3} ($P_{O2} = 1$ Pa and $T_s = 400$ °C); such a discovery was in good agreement with equation (1).

Figure 5(b) exhibits the reflectance (solid lines) and absorption (broken lines) of ITO films influenced by substrate temperature (400 °C to 100 °C); P_{O2} was set to 1 Pa. The match between the blue and red lines (solid or broken) represents the similarity of the optical properties of ITO films deposited at $T_s = 300$ °C and $T_s = 400$ °C. This observation could also be supported by the identical microstructure in XRD patterns and electrical results. The ITO film with $T_s = 200$ °C also had the same behavior except for relatively high absorptions. However the sample deposited with $T_s = 100$ °C presented very high absorptances (low reflectances) in the range

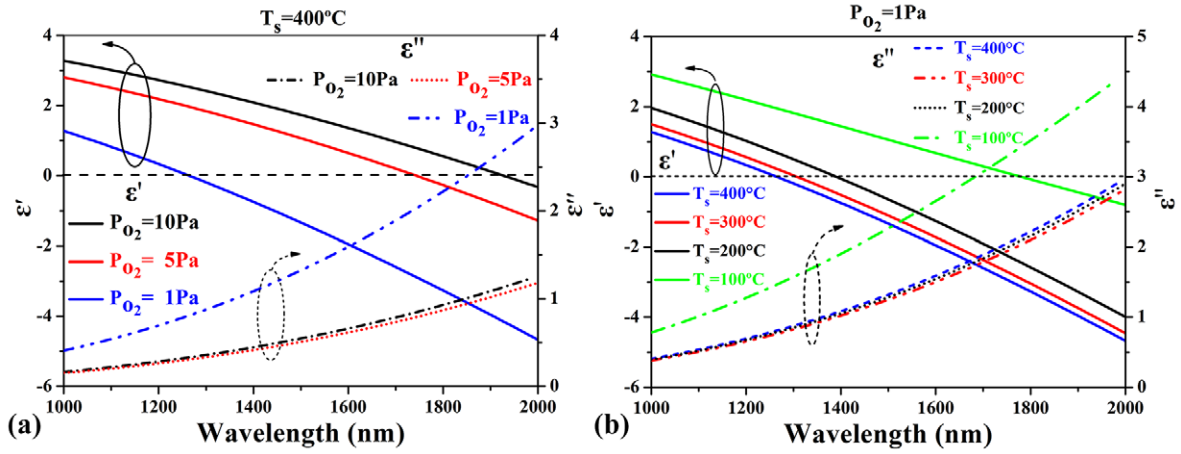

Figure 6. (a) Fitted ε' (real part) and ε'' (imaginary part) permittivity of ITO films as a function of oxygen pressure (black line, 10 Pa; red line, 5 Pa; blue line, 1 Pa); the substrate temperature was 400 °C. (b) Fitted ε' (real part) and ε'' (imaginary part) permittivity of ITO films as a function of substrate temperature (blue line, 400 °C; red line, 300 °C; black line, 200 °C; green line, 100 °C); the oxygen pressure was 1 Pa. The black straight dashed line in each figure was drawn as a sign to show where ε' changed from positive to negative.

of 1500–2500 nm, which was quite different from the other three samples. Such a phenomenon may result from both the amorphous property of the ITO film and the excess number of oxygen vacancies.

In order to evaluate the plasmonic property of ITO films in the near IR, spectroscopic ellipsometry (SE) was applied to measure the amplitude ratio (Ψ) and the phase difference (Δ) when incident light (wavelength range from 1000 nm to 2000 nm) interacted with ITO films at an angle of 58°. Then an optical model was applied to retrieve the dielectric constant of the ITO film. Many works have been done to explore the optical property of ITO films using SE method by exclusively using the Drude and Lorentz model or Cauchy model to describe the optical constant of the ITO film in the visible range [34, 48–50]. Here the Drude model [35, 51] was used to describe the metallic property of ITO films in the near-IR range (regardless of the interband absorption described by the Lorentz model in the UV range) and defined as follows:

$$\varepsilon(\omega) = \varepsilon'(\omega) + \mathrm{i}\,\varepsilon''(\omega) = \varepsilon_\infty - \frac{\omega_\mathrm{p}^2}{\omega\,(\omega + \mathrm{i}\,\Gamma)} \tag{2}$$

$$\varepsilon'(\omega) = \varepsilon_\infty - \frac{\omega_\mathrm{p}^2}{\omega^2 + \Gamma^2} \tag{3}$$

$$\varepsilon''(\omega) = \frac{\omega_\mathrm{p}^2 \Gamma}{\omega^3 + \omega^2 \Gamma^2}. \tag{4}$$

Here, ω_p is the plasma frequency as defined in equation (1), ε_∞ the high frequency dielectric constant, ω the frequency of the free space wave and Γ the Drude relaxation rate, which was responsible for scattering/ohmic losses [10].

Figure 6(a) shows the ε' (real part) and ε'' (imaginary part) permittivity of ITO films as a function of oxygen pressure (black line, 10 Pa; red line, 5 Pa; blue line, 1 Pa); $T_\mathrm{s} = 400$ °C. The straight black dashed line is presented to show the crossover wavelength (λ_c), which was defined as the wavelength where ε' (real part) changed from positive to negative.

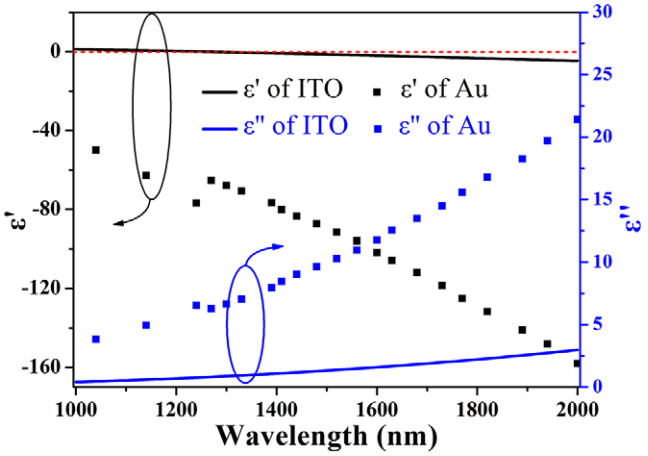

Figure 7. Comparison between permittivity (lines) of ITO film ($P_{O2} = 1$ Pa and $T_\mathrm{s} = 400$ °C) and permittivity (dots) of Au [52] reported by Plik *et al*.

The ε' of ITO film deposited with $P_{O2} = 10$ Pa remained positive until the wavelength reached 1930 nm, while the λ_c values of ITO films deposited with $P_{O2} = 5$ Pa and $P_{O2} = 1$ Pa were 1750 nm and 1270 nm, respectively. $\lambda_\mathrm{c} = 1270$ nm was shorter than that (1.4–1.5 μm) of reported AZO film [26], indicating that the ITO film can be used as a plasmonic material in applications whose operating wavelength is 1.55 μm. The shifting of λ_c to shorter wavelength was linearly related to the decrease of P_{O2}, which can be explained according to the Hall measurement results (shown in table 1): carrier concentration increased from 2.85×10^{20} ($P_{O2} = 10$ Pa) to 1.34×10^{21} cm^{-3} ($P_{O2} = 1$ Pa). According to equations (1) and (3), the enlarged N contributed to a larger ω_p, making it easier for ε' to be negative. According to Naik *et al* [10], a large ε'' was obtained by either large Γ (intense grain-boundary scattering) or large N, or both. Thus in our case the ITO film with the highest carrier concentration (1.34×10^{21} cm^{-3} for $P_{O2} = 1$ Pa) exhibited the largest ε'' (<3) compared with ε'' (<1.5) of the other two samples. The nearly identical ε'' of ITO films

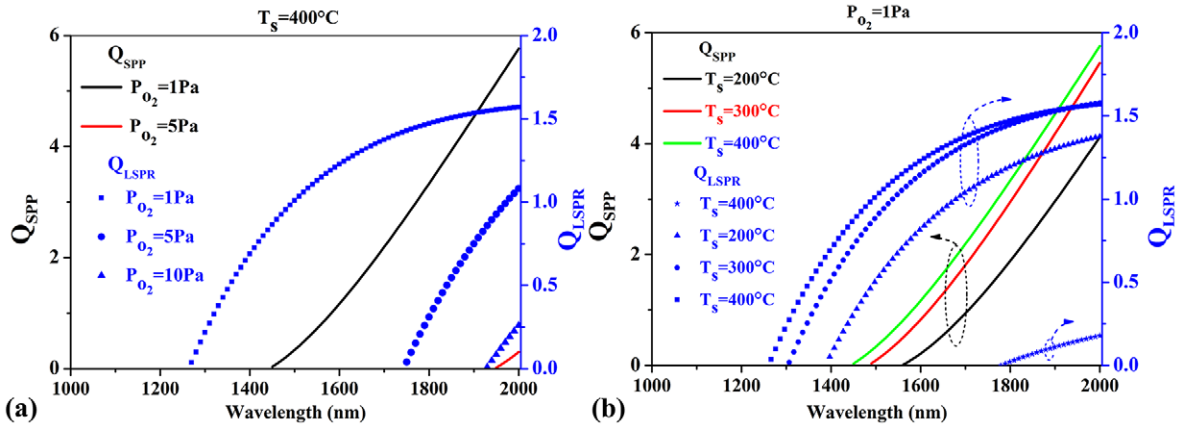

Figure 8. (a) Quality factors of ITO films with fixed substrate temperature (400 °C) for localized surface plasmon resonances (Q_{LSPR}, solid lines) and surface plasmon polaritons (Q_{SPP}, scatter points: ■, ●, ▲). (b) The corresponding quality factors (Q_{LSPR}, solid lines; Q_{SPP}, scatter points) for ITO films with fixed oxygen pressure (1 Pa).

with $P_{O2} = 10$ Pa and $P_{O2} = 5$ Pa was probably influenced by Γ, as the XRD patterns were nearly the same and exhibited good polycrystallinity, as shown in figure 1(a).

Figure 6(b) shows the evolution of permittivity (ε' and ε'') according to the change of substrate temperature (blue, $T_s = 400$ °C; red, $T_s = 300$ °C; black, $T_s = 200$ °C; green, $T_s = 100$ °C) when oxygen pressure was kept at 1 Pa. Aided by the straight dashed line, the shifting of λ_c to shorter wavelength according to the increase of T_s from 100 to 400 °C can be clearly observed. The λ_c of the ITO films with $T_s = 100$ °C was 1780 nm, which was larger than that ($\lambda_c = 1400$ nm at $T_s = 200$ °C, $\lambda_c = 1310$ nm at $T_s = 300$ °C, $\lambda_c = 1270$ nm at $T_s = 400$ °C) of ITO films with higher substrate temperatures. Still the ITO film deposited with $T_s = 400$ °C and $P_{O2} = 1$ Pa has the shortest λ_c with permittivity at 1.55 μm of $\varepsilon = -1.6401 + i\,1.4532$; the negative ε' made it possible for ITO films to act as alternative plasmonic materials in the near-IR range. From figure 6(b), the ε'' of the ITO sample deposited under $T_s = 100$ °C was much larger than that of the other samples; this was mainly due to the intense grain boundary scattering (this can be seen from the XRD pattern shown in figure 1(d)). As ε'' was proportional to N (equation (4)) and relaxation rate Γ ($\Gamma = e/\mu m^*$) [10], the less polycrystalline microstructure of the $T_s = 100$ °C ITO sample detrimentally influenced the Hall mobility and increased the relaxation rate Γ. The nearly identical ε'' for T_s values of 200 °C, 300 °C, and 400 °C showed that ε'' was less sensitive to substrate temperature. The carrier concentrations of the three samples were all above 1×10^{21} cm^{-3} and the XRD pattern showed that they were all polycrystalline (especially for $T_s = 300$ °C and $T_s = 400$ °C).

Figure 7 shows a comparison between the permittivity (lines) of the ITO sample ($T_s = 400$ °C, $P_{O2} = 1$ Pa) and that (dots) of gold [52] by Palik *et al.* It is obvious that the value of ε' (1.6401 @ 1.55 μm) of ITO was much smaller than that (95.62 @ 1.55 μm) of gold. For ε'', the ITO film showed its advantages: $\varepsilon''_{ITO} = 1.4532$ of the ITO film was several times lower than $\varepsilon''_{Au} = 10.96$ of gold at a wavelength of 1.55 μm. The small imaginary part of the permittivity of the ITO film indicated the possibility of lowering optical losses as well as improving the working efficiency in the near-IR range.

In order to evaluate the plasmonic properties of the ITO films, two kinds of quality factor were introduced in the applications of localized surface plasmon resonances (LSPRs) and surface plasmon resonances (SPPs) [13]. The two quality factors were defined as follows:

$$Q_{LSPR}(\omega) = \frac{-\varepsilon'_m(\omega)}{\varepsilon''_m(\omega)} \tag{5}$$

$$Q_{SPP}(\omega) = \frac{\varepsilon'_m(\omega) + \varepsilon_d(\omega)}{\varepsilon'_m(\omega)\varepsilon_d(\omega)} \frac{\varepsilon'_m(\omega)^2}{\varepsilon''_m(\omega)}. \tag{6}$$

Here $\varepsilon_m(\omega)$ is the permittivity of the plasmonic material, i.e. ITO. $\varepsilon_d(\omega)$ is the permittivity of the surrounding dielectrics; here air was chosen with $\varepsilon_d(\omega) = 1$.

Figure 8 illustrates the Q_{LSPR} (dots) and Q_{SPP} (lines) of ITO samples as a function of deposition conditions, (a) for varied P_{O2} with fixed $T_s = 400$ °C and (b) for varied T_s with fixed $P_{O2} = 1$ Pa. In the two figures, the Q_{SPP} of ITO deposited with $P_{O2} = 10$ Pa, $T_s = 400$ °C, and $P_{O2} = 1$ Pa, $T_s = 100$ °C, did not exist because $\varepsilon'_m(\omega) + 1 > 0$ in the range 1000–2000 nm. As can be seen from figure 8(a), Q_{LSPR}/Q_{SPP} were highly dependent on the oxygen pressure, and the ITO sample deposited with $P_{O2} = 1$ Pa, $T_s = 400$ °C, presented the best performance. Meanwhile, from figure 8(b), it seems that when the oxygen pressure was kept at 1 Pa the substrate temperature cast less influence on Q_{LSPR}/Q_{SPP}, especially when $T_s \geqslant 200$ °C. At the wavelength of 1.55 μm the Q_{LSPR} and Q_{SPP} of the ITO film with $P_{O2} = 1$ Pa, $T_s = 400$ °C, were 1.128 and 0.722, which were much smaller than those of gold ($Q_{LSPR} = 10.63$, $Q_{SPP} = 1140$) [13]. However, for applications of transformation optics (TO: require a negative but small in magnitude ε') [13], the quality factor was $\varepsilon''_m(\omega)^{-1}(-\varepsilon'_m(\omega) \sim \varepsilon_d(\omega) \sim 1)$. Thus in this case noble metals like such as gold or silver were not suitable at all because of their large magnitude of ε' and ε'' in the near-IR.

4. Conclusions

The influences of substrate temperature and oxygen pressure on the microstructures and electrical and optical properties of

ITO films prepared by pulsed laser deposition have been systematically explored and discussed. By increasing substrate temperature (to 400 °C) and decreasing oxygen pressure (to 1 Pa), the highest carrier concentration was obtained at the level of 1.34×10^{21} cm^{-3}. Such a high carrier concentration resulted in the shifting of λ_c as low as 1270 nm while obtaining a permittivity of $\varepsilon_{ITO} = -1.6401 + i\ 1.4532$ at the wavelength of 1.55 μm. As compared with the permittivity of gold ($\varepsilon_{Au} = -95.62 + i\ 10.96$ @ 1.55 μm), the small magnitude of both the real and imaginary parts of the permittivity of ITO provided advantages in applications of transformation optics and others. Besides, the properties of ITO films can be tuned according to the deposition conditions, making the choice of ITO films more flexible. Furthermore, the stable chemical and physical properties of ITO films would be useful in some extreme applications where conventional noble metals are not suitable. All the results and discussion indicate that ITO films are qualified to replace conventional metals for low loss alternative plasmonic materials in the near-IR range.

Acknowledgment

This research was supported by the National Basic Research Program of China (973 Program, No 2013CB632104), the National Natural Science Foundation of China (No 61575176), the Natural Science Foundation of Zhejiang Province of China (No LZ12F04002) and the Research Foundation of State Key Laboratory of Modern Optical Instrumentation (moi20150105). In addition, financial support by The Hong Kong Polytechnic University (grant A-PL21/A-PM51) is acknowledged.

References

[1] Willets K A and Duyne R P V 2007 *Annu. Rev. Phys. Chem.* **58** 267–97
[2] Anker J N, Hall W P, Lyandres O, Shah N C, Zhao J and Duyne R P V 2008 *Nat. Mater.* **7** 442–53
[3] Leong E S P, Wu S J, Zhang N, Loh W W, Khoo E H, Si G Y, Dai H T and Liu Y J 2014 *Nanotechnology* **25** 055203
[4] Valentine J, Zhang S, Zentgraf T, Ulin-Avila E, Genov D A, Bartal G and Zhang X 2008 *Nature* **455** 376–9
[5] Hokari R, Kanamori Y and Hane K 2014 *Opt. Express* **22** 3526–37
[6] Soukoulis C M and Wegener M 2011 *Nat. Photonics* **5** 523–30
[7] Gramotnev D K and Bozhevolnyi S I 2010 *Nat. Photonics* **4** 83–91
[8] Abb M, Albella P, Aizpurua J and Muskens O L 2011 *Nano Lett.* **11** 2457–63
[9] Szunerits S, Castel X and Boukherroub R 2008 *J. Phys. Chem. C* **112** 15813–7
[10] Naik G V, Shalaev V M and Boltasseva A 2013 *Adv. Mater.* **25** 3264–94
[11] Kildishev A V and Shalaev V M 2008 *Opt. Lett.* **33** 43–5
[12] Khurgin J B and Boltasseva A 2012 *MRS Bull.* **37** 768–79
[13] West P R, Ishii S, Naik G V, Emani N K, Shalaev V M and Boltasseva A 2010 *Laser Photonics Rev.* **4** 795–808
[14] Grill A, Kane W, Viggiano J, Brady M and Laibowitz R 1992 *J. Mater. Res.* **7** 3260–5
[15] Peng K, Lu A, Zhang R and Lee S T 2008 *Adv. Funct. Mater.* **18** 3026–35
[16] Ellmer K 2012 *Nat Photonics* **6** 809
[17] Ginley S D, Perkins D J 2010 Transparent conductors *Handbook of Transparent Conductors* ed S D Ginley (London: Springer) pp 1–25
[18] Kim J, Zhao Y, Naik G V, Emani N K, Guler U, Kildishev A V, Alu A and Boltasseva A 2013 Nanostructured transparent conductive oxide films for plasmonic applications *Conf. on Lasers and Electro-Optics*
[19] Naik G V, Liu J, Kildishev A V, Shalaev V M and Boltasseva A 2012 *Proc. Natl Acad. Sci.* **109** 8834–8
[20] Losego M D, Efremenko A Y, Rhodes C L, Cerruti M G, Franzen S and Maria J P 2009 *J. Appl. Phys.* **106** 024903
[21] Michelotti F, Dominici L, Descrovi E, Danz N and Menchini F 2009 *Opt. Lett.* **34** 839–41
[22] Rhodes C, Franzen S, Maria J P, Losego M, Leonard D N, Laughlin B, Duscher G and Weibel S 2006 *J. Appl. Phys.* **100** 054905
[23] Hibbins A P, Sambles J R and Lawrence C R 1998 *J. Mod. Opt.* **45** 2051–62
[24] Chen N C, Lien W C, Liu C R, Huang Y L, Lin Y R, Chou C, Chang S Y and Ho C W 2011 *J. Appl. Phys.* **109** 043104–7
[25] Naik G V, Schroeder J L, Ni X, Kildishev A V, Sands T D and Boltasseva A 2012 *Opt. Mater. Express* **2** 478–89
[26] Kim H, Osofsky M, Prokes S M, Glembocki O J and Piqué A 2013 *Appl. Phys. Lett.* **102** 171103
[27] Ohta H, Orita M, Hirano M, Tanji H, Kawazoe H and Hosono H 2000 *Appl. Phys. Lett.* **76** 2740–2
[28] Park D G *et al* 2001 Robust ternary metal gate electrodes for dual gate CMOS devices *Electron Devices Meeting. Technical Digest Int.* (Piscataway, NJ: IEEE) pp 30.6.1–4
[29] Fortunato E *et al* 2008 *Sol. Energy Mater. Sol. Cells* **92** 1605–10
[30] Rhodes C, Cerruti M, Efremenko A, Losego M, Aspnes D, Maria J P and Franzen S 2008 *J. Appl. Phys.* **103** 093108
[31] Franzen S, Rhodes C, Cerruti M, Gerber R W, Losego M, Maria J P and Aspnes D 2009 *Opt. Lett.* **34** 2867–9
[32] Franzen S 2008 *J. Phys. Chem.* C **112** 6027–32
[33] Melikyan A *et al* 2011 *Opt. Express* **19** 8855–69
[34] Kim J, Naik G V, Emani N K and Boltasseva A 2012 *IEEE J. Sel. Top. Quantum Elec.* **19** 4601907
[35] Feigenbaum E, Diest K and Atwater H A 2010 *Nano Lett.* **10** 2111–6
[36] Kim S H, Park N M, Kim T Y and Sung G Y 2005 *Thin Solid Films* **475** 262–6
[37] Kim H, Pique A, Horwitz J, Mattoussi H, Murata H, Kafafi Z and Chrisey D 1999 *Appl. Phys. Lett.* **74** 3444–6
[38] Thilakan P, Minarini C, Loreti S and Terzini E 2001 *Thin Solid Films* **388** 34–40
[39] Kim H, Gilmore C M, Pique A, Horwitz J S, Mattoussi H, Murata H, Kafafi Z H and Chrisey D B 1999 *J. Appl. Phys.* **86** 6451–61
[40] Lowndes D H, Geohegan D B, Puretzky A A, Norton D P and Rouleau C M 1996 *Science* **273** 898–903
[41] Willmott P R and Huber J R 2000 *Rev. Mod. Phys.* **72** 315
[42] Aziz M J 2008 *Appl. Phys.* A **93** 579–87

[43] Kim H S 2007 Transparent conducting oxide films *Pulsed Laser Deposition of Thin Films: Applications-Led Growth of Functional Materials* ed R Eason (Hoboken, NJ: Wiley) pp 239–60
[44] Petukhov I A *et al* 2012 *Inorg. Mater.* **48** 1020–5
[45] Najwa S *et al* 2014 *Superlattices Microstruct.* **72** 140–7
[46] Minami T 2005 *Semicond. Sci. Technol.* **20** S35
[47] Coutts T J, Young D L and Gessert T A 2010 Modeling characterization, and properties of transparent conducting oxides *Handbook of Transparent Conductors* ed S D Ginley (London: Springer) pp 51–110
[48] Lohner T, Kumar K J, Petrik P, Subrahmanyam A and Bársony I 2014 *J. Mater. Res.* **29** 1528–36
[49] Woollam J A, McGaham W and Johs B 1994 *Thin Solid Films* **241** 44–6
[50] Jung Y S 2004 *Thin Solid Films* **467** 36–42
[51] Fang X, Mak C L, Dai J Y, Li K, Ye H and Leung C W 2014 *ACS Appl. Mater. Interfaces* **6** 15743–52
[52] Lynch D W and Hunter W R 1998 Comments on the optical constants of metals and an introduction to the data for several metals *Handbook of Optical Constants* ed E D Palik (San Diego: Academic) pp 275–383